Clogging and unclogging of hydrocarbon-contaminated nanochannels

Reference:
Javdani Z., Hassani N., Faraji Fahim, Zhou R., Sun C., Radha B., Neyts Erik, Peeters François, Neek-Amal M..- Clogging and unclogging of hydrocarbon-contaminated nanochannels
The journal of physical chemistry letters / American Chemical Society - ISSN 1948-7185 - Washington, Amer chemical soc, 13:49(2022), p. 11454-11463
Full text (Publisher's DOI): https://doi.org/10.1021/ACS.JPCLETT.2C03016
To cite this reference: https://hdl.handle.net/10067/1928150151162165141

Clogging/Unclogging of Hydrocarbon Contaminated Nanochannels

Z. Javdani,[†] N. Hassani,[†] F. Faraji,[‡] R. Zhou,[§] C. Sun,[§] B. Radha,[‖] E. Neyts,[‡] F. M. Peeters,[¶] and M. Neek-Amal[*,#]

†*Department of Physics, Shahid Rajaee University, 16875-163 Lavizan, Tehran, Iran.*

‡*PLASMANT, Department of Chemistry, University of Antwerp, Universiteitsplein 1, 2610 Antwerp, Belgium.*

¶*Department of Physics, Universiteit Antwerpen, Groenenborgerlaan 171, B-2020 Antwerpen, Belgium.*

§*State Key Laboratory of Multiphase Flow in Power Engineering, Xi'an Jiaotong University, China.*

‖*Department of Physics and Astronomy, School of Natural Sciences, The University of Manchester, and National Graphene Institute, Oxford Road, Manchester M13 9PL, UK.*

⊥*Departamento de Física, Universidade Federal do Ceará, 60455-760 Fortaleza, Ceará, Brazil.*

#*Department of Physics, Shahid Rajaee Teacher Training University, 16875-163 Lavizan, Tehran, Iran.*

E-mail: mehdi.neekamal@gmail.com

Abstract

Angstrom-scale channels made from 2D materials have received a lot of attention in nanofluidics. The recent advantages of the fabrication of artificial nanochannels enabled new research on molecular transport, permeance, and selectivity of various gas and

molecules. However, the physisorption/chemisorption of the unwanted molecules (usual hydrocarbons) inside nanochannels results in the alteration of nanochannels functionality. We investigate contamination, due to hydrocarbon molecules, nanochannels made of graphene, hexagonal boron nitride (hBN), BC_2N, and molybdenum disulfide (MoS_2) using molecular dynamics simulations. Nanochannel height is found to play a crucial role in the clogging/unclogging of the nanochannel. We found that for a certain size of nanochannel, i.e. h=0.7 nm, as a result of anomalous hydrophilic nature of nanochannels made of graphene [Li *et al.*, *Nat. Mater.* **2013**, *12*, 925-931.], the hydrocarbons are fully adsorbed in nanochannel, giving rise to full uptake. Increasing temperature plays an important role in unclogging, while pressure does not have a significant role. As a pioneer work, our results contribute to a better understanding and highlighting the important factors of nanochannel's alleviating the contamination and unclogging which are in good agreement with recent experiments [Sajja *et al.*, *Nanoscale* **2021**, *13*, 9553-9560].

KEYWORDS: ***Nanofluidics, Hydrocarbon contamination, Nanochannel, Clogging/Unclogging***

I. INTRODUCTION

Fluids confined in angstrom scale channels exhibit very different properties than those in micro channels, such as electro-osmotic flow, high viscosity, small dielectric constants, and small ion enrichment/depletion.[1] These differences result from various types of forces that can influence fluid transport through nanochannels.[2]

The recent advances in nanofabrication have enabled fluidic devices with capillaries at the molecular scale.[3–13] Angstrom scale channels mainly made of two-dimensional (2D) materials have emerged as promising devices for molecular filtration and separation.[14,15] Despite promising applications, there are major challenges that limit the use of 2D materials in nanofluidics. As an example, contamination by airborne particles can adsorb onto

the hydrophilic surfaces of 2D materials, altering the surface properties and contaminating nanochannels.[16] In fact, when nanochannels are reduced to angstrom sizes, clogging occurs from contamination adhering to them.[17] At the angstrom scale, the interaction between contaminants and the nanochannel wall becomes more significant. Adsorption of contaminants onto the wall of the nanochannel occurs as a result of this interaction which hinders the permeation of fluid in the channel. Due to the practical difficulty of evaluating contamination within strong confinement, the effects of contamination on confined nanochannels remain largely unexplored.[18] It is therefore important to study the influence of contamination of the surface of 2D materials, including wetting of the surfaces, modification of the concentration of local charge carriers[16,19–21] in the confining walls.

Although airborne hydrocarbon contamination is in general very low, experiments nevertheless have found that surface contamination mainly includes hydrocarbons.[22] At present, there is very little literature (either experimental or theoretical) on hydrocarbons in the presence of confinement.[23–25] Single-wall carbon nanotubes (SWCNTs) were reported to be able to efficiently separate n-hexane from cyclohexane. The van der Waals pore size of SWCNTs was 0.42 nm, which was smaller than the kinetic diameter (k_d) of both molecules. They explained the mechanism of entry of large molecules into a narrow channel using *ab initio* molecular dynamics simulations, in which n-hexane (C_6h_{14}) molecules were stretched by approximately 11.2% to enter the narrow pores of the nanotubes.[24]

In a recent experiment with graphene and hexagonal boron nitride (hBN) nanochannels the effect of hydrocarbons on the flow of He gas was investigated.[17] Blocking and reduction of helium gas flow was detected as a sign of hexane contamination within confined nanochannels with heights of 0.4 nm, 0.7 nm and 1.7 nm.[17] After introducing hexane into a 1.7 nm thick nanochannel, the helium flow decreased by about three orders of magnitude. This was followed by a heat treatment of 150 C° for 20 minutes, which led to the recovery of the He flow in the nanochannel. Also, it was reported that an interaction between the nanochannel wall and the long alkyl chain completely blocked the nanochannel when the channel has

a height of 0.7 nm, and neither helium flushes nor heat treatments were able to unclog it. The physics behind this phenomena and a detailed quantitative analysis of hydrocarbon contamination in confined areas remains is the topic of the present paper. We will show the importance of slit height on the effect of clogging of such channels and investigate of the material of the channel walls has any effect.

II. MODELS

Here, we will use molecular dynamics (MD) simulations to study various aspects of the problem. In particular, we investigate hydrocarbon contamination and permeation through nanochannels made of graphene, hBN, BC_2N, and molybdenum disulfide (MoS_2). In order to thoroughly analyze the nanochannel contamination. We study the effects of the concentration of hydrocarbon and helium on the clogging of channels having different heights as well as analyze the interaction energy between hydrocarbon and nanochannels wall. It's vital to look at the possibility of particles entering the nanochannel before looking into the process of particle flow inside the channel. As a result, two separate models were employed in this paper.

II.a. Model-I. The first model looks into the probability of particle entrance using the interaction of the hexane/cyclohexane molecule with different channels. Here we ignore the helium gas. We simply considered a simulation setup for the movement of a hexane (C_6H_{14})/cyclohexane (C_6H_{12}) molecule through different nanochannels (hBN, graphene, and MoS_2) which for hBN and MoS_2 are illustrated in Figure 1. First, the hexane molecule was gradually moved towards entering and passing through the nanochannel and the potential energy of the system was calculated as the hexane was moving (see Figure 1(a)). The calculations were performed for channels with different heights ranging from h $\approx$ 0.4 nm to 2 nm (along z-direction). The nanochannels are 6 nm long (along x-direction).

The simulation box axial domain was limited to the nanochannel length with periodic

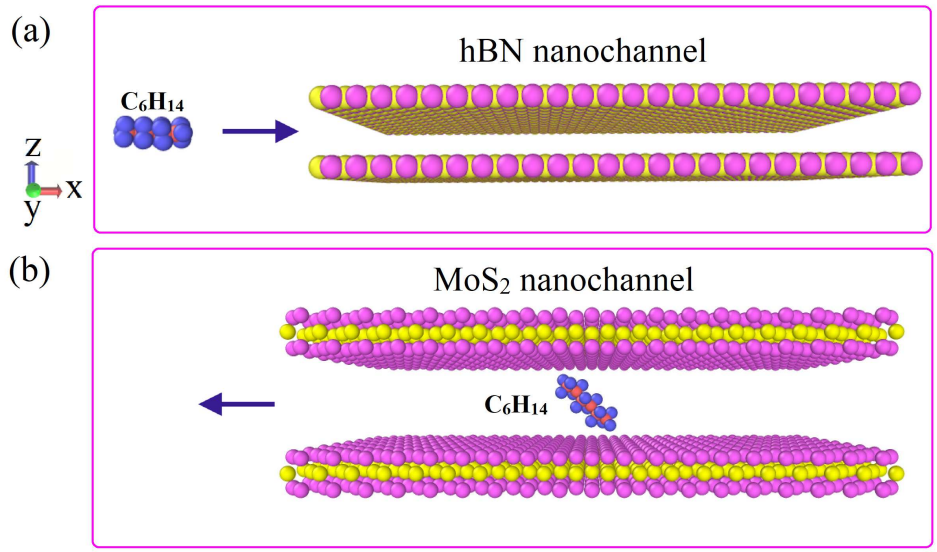

Figure 1: Model I-(a) Schematic of the simulation setup for hBN nanochannel. The hexane molecule is gradually moved towards entering and passing through the channel and the system potential energy is examined as function of the position of hexane. The calculations are repeated for graphene and MoS_2 nanochannels for different channel heights from 0.4 nm to 2 nm and (b) the simulation setup for MoS_2 nanochannel. The arrow in (a) and (b) refers to the penetration and existing of hexane from the channel, respectively.

boundary condition. The nanochannel height was increased with 0.5 nm steps and the simulation was performed for each height until the potential energy of the system reached a steady state. We also simulated the hexane inside the widening MoS_2 nanochannel (see Figure 1(b)).

II.b. Model-II. The second model which is more close to the actual experiment, relevant to the experiment looks into the mechanism of particle flow and clogging in the nanochannels. In the second model, the permeation of hydrocarbon molecules (here hexane) and He atoms simultaneously are investigated for different height of nanochannels made of graphene, hBN, BC_2N and MoS_2 which are called G-NCs, hBN-NCs, BC_2N-NCs, and MoS_2-NCs, respectively. Figure 2 shows the schematic of the simulation setup containing 200 He atoms and 200 hexane molecules. The left and right boxes are called feed reservoirs (FR) and exit reservoirs (ER), respectively.

In the initial step, 200 He atoms are placed in the left box, and after reaching equilibrium

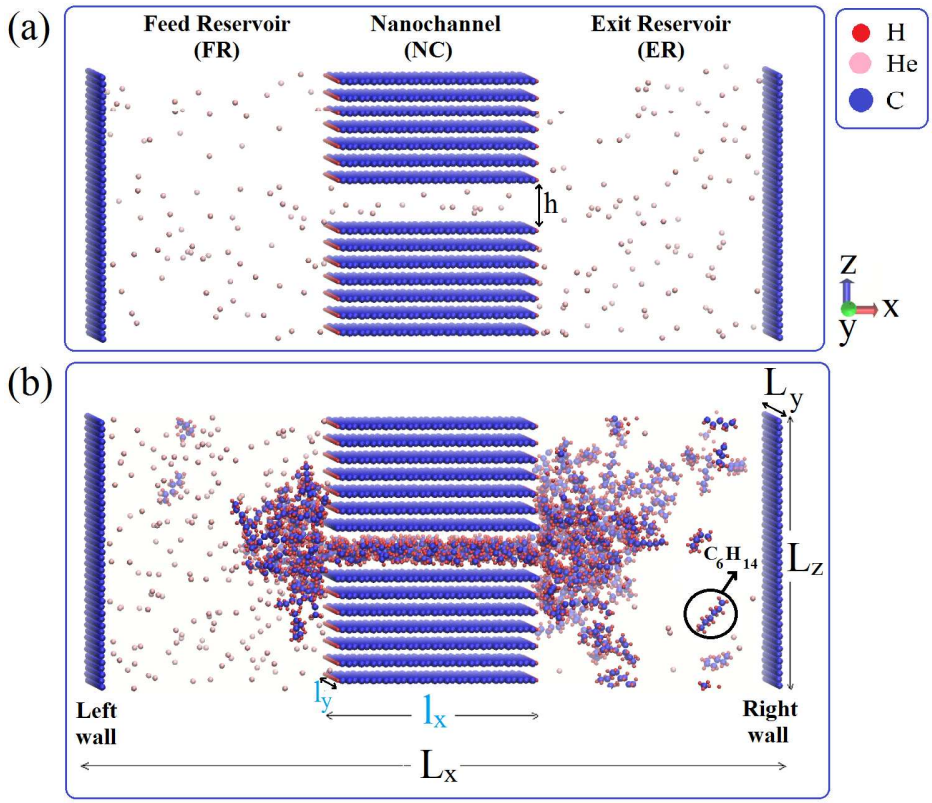

Figure 2: Model II-Schematic of the simulation setup for (a) permeation through graphene nanochannel (G-NC) which contains 200 He atoms and (b) contamination of graphene nanochannel (G-NC) which contains 200 He atoms and 200 hexane molecules.

shown in Figure 2(a), certain number of hexane molecules (50, 100, 150, and 200) are added to the left box. After reaching equilibrium we counted hexane molecules in eah region.

On the left and right sides of the simulation box, we placed graphene walls which allow us to apply pressure. By moving both walls to the right side of the simulation box, a uniform pressure gradient can be applied throughout the simulation box while the volume of the simulation box remained unchanged. The length (L_x), width (L_y) and height (L_z) of the simulation box are 20 nm, 4.3 nm and 5.4 nm, respectively. The flow direction (x) is along the simulation box (L_x), where the nanochannel height (h), the vertical distance between the two sheets, is parallel to the z-axis. In this model, the effect of the nanochannel height is also studied by removing n (n=1 to 5) sheets from a layered structure containing N_L sheets, where N_L is sixteen for graphene, hBN, BC_2N and N_L is taken eight for MoS_2. The

layers at the top and bottom of the nanochannel are kept rigid. The origin of the coordinate axis coincides with the center of the nanochannels. The length (l_x) and width (l_y) of the nanochannels are 4 nm and 4.3 nm, respectively.

III. RESULTS AND DISCUSSION

Different parameters can affect hexane penetration or clogging nanochannels, including the energy barrier for the hydrocarbon to enter the nanochannel, density of hydrocarbon, size and material of nanochannel walls.[17,25] For example, for nanochannels with a height of 1.7 nm, it is shown that the flow rate of He inside the G-NC and the hBN-NC are two orders of magnitude larger than those of MoS_2-NC.[25] This is due to specular surface scattering that results in ballistic transport and friction-less gas movement. These studies show that nanochannel materials can affect gas flow. Here we explore different aspect of the problem using the two aformentioend models.

III.a. The energy barrier (model I). In order to get deeper physical insight in the clogging mechanism and to be able to explain the recent experiment,[17] we calculate the energy barrier for the hydrocarbon to enter the nanochannel as function of the width of the 2D channel. Once inside the channel we obtain the diffusion barrier for the hydrocarbon to move inside the channel.

In our first simulation model (see Figure1), we exposed the 2D nanochannels made of graphene, hBN, as well as MoS_2 walls with a hexane molecule as a representative of hydrocarbon contamination. Figure 3 illustrates the variation of the potential energy for graphene, hBN and MoS_2 nanochannel. The channel's entrance is located at $x = 0$. When the nanochannel height is small (h < 0.7 nm), there is an energy barrier ($E > 0$) against hexane (or cyclohexane) entering the channel (see panel a-c of Figure 3). In wide channels (h ≥ 0.7 nm), on the other hand, there is no energy barrier ($E < 0$), but it is energetically favorable for hexane to enter the channel (panel d-f of Figure 3). Notice that there is a

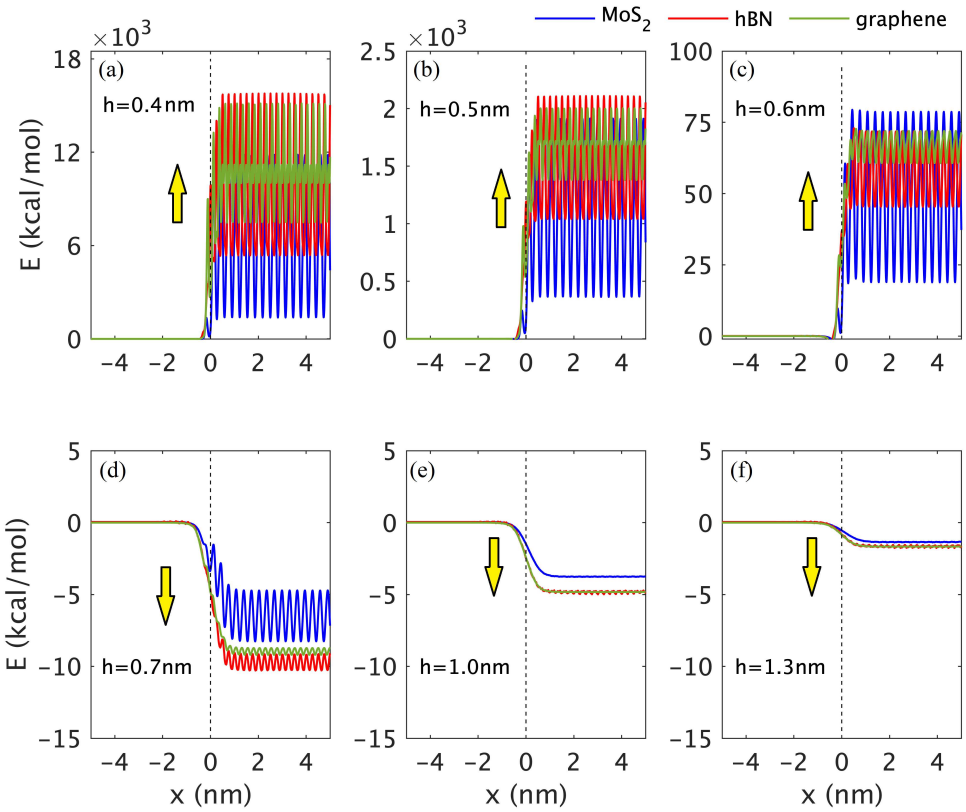

Figure 3: Variation of the system potential energy as the hexane molecule approaches and passes through the graphene, hBN and MoS_2 nanochannels for different channel heights. The arrows in (a-c)/(d-f) indicate the decreasing/increasing of the potential energy when hydrocarbon is entered to the channel.

capillary-like hexane absorption in the nanochannels. By comparing the potential energy results, one can distinguish a critical height, which for all nanochannel potentials is between 0.6 nm and 0.7 nm which separates two distinct barrier and adsorption regimes. This is compatible with the experiment for ultra slim channels (0.4 nm), i.e. where no clogging of the nanochannels is observed.[17] Accordingly, the energy barrier prevents any penetration of hydrocarbon and thus clogging of the nanochannel. Three regimes can be distinguished: 1) h $<$ 0.64 nm when hydrocarbons (hexane) cannot enter the channel, 2) for h $=$ 0.7 nm there is maximum binding of the hydrocarbons inside the channel making unclogging almost impossible, and 3) h $\geq$ 1 nm when the hydrocarbons are weakly bound to one of the channel walls and unclogging by high temperature annealing can be realised.

As shown in Figure 3, energy shows oscillations (ΔE is the amplitude of these oscilations) and this is an indicative measure of the difficulty in hydrocarbon unclogging of the nanochannels. For those nanochannels where there are large energy fluctuations, the hexane has to overcome local potential barriers induced by the walls to get out of the nanochannel. This also agrees well with experiment that wide channels could be unclogged using He flushing.[17] The results for energy barrier against movement of cyclohexane molecule where it approaches and passes through the graphene, hBN and MoS_2 nanochannels for different channel heights is presented in Figure S1 which is qualitatively similar to our results.

III.b. The h =0.4 nm graphene nanochannel (model II).

Here, we considered a graphene nanochannel (G-NC) with a height of 0.4 nm and investigate the permeation of hexane molecules and He atoms through it using model II. The hexane molecule (without deformation) cannot enter the nanochannels because its kinetic diameter (k_d) exceeds height of the nanochannel. Consequently, hexane molecules with k_d=0.43 nm can only penetrate the channels with h> 0.43 nm.[26] Notice that, Qu *et al.*[24] observed the penetration of a hexane molecule via a nanochannel with h = 0.4 nm. They explained this observation through the deformation and elongation of the hexane molecule. Our simulation and recent experiment[17] show do not confirm penetration of hexane molecule.

III.c. The h =0.7 nm graphene nanochannel (model II).

Next, we present the results for the most interesting case, i.e., the nanochannel with a height of 0.7 nm, to explore the effect of hydrocarbon adsorption inside the channel in the presence of helium gas which is a realistic model mimicking experimental setup. To simulate the 0.7 nm nanochannel, two graphene sheets (n=2) are extracted from the layered graphene structure. In fact, a key factor that controls clogging of nanochannels is the density of hydrocarbon molecules. This parameter is investigated specifically for graphene nanochannel with h=0.7 nm, and then generalized to the other nanochannels made of MOS_2 and hBN and BC_2N.

As mentioned already, the FR region is first filled with 200 He atoms and allowed the

whole system to relax at room temperature. Then, the number of He atoms in FR, ER and G-NC regions are counted and used as the initial number (N_0) of He in each region (see Figures 4 and S2; black curves). One naturally expects to see $N_0(FR) \approx N_0(ER)$ for helium after reaching thermodynamics equilibrium. Next, we added certain number (50, 100, 150, and 200) of hexane molecules to the FR which enabled us to quantify the clogging/unclogging process within the nanochannel. Then we allow the whole system to relax. We compare the number of He atoms in each region with N_0. The deviation of the number of He in each region with respect to N_0 helps us to study the migration of He from each region, thus it provides insights about clogging/unclogging. The corresponding results for time evolution of He and hexane are shown in Figures 4 and 5, respectively.

Interestingly, when the initially 50 number of hexane is added to FR, during time up to 5 ns, almost all the hexane molecules enter the G-NC and stay there (full uptake, see Figure 5a, black curve), i.e. there is no existing hexane into the ER. The latter is consistent with our findings in Figure 3, where we found maximum binding of the hydrocarbons inside the h=0.7 nm channel. Therefore, h≈0.7 nm is a critical channel height.

The results for other number of hexane molecules (i.e. 100 and 200 hexane molecules in the FR) are more or less the same: after 5 ns at 300 K, around only 30% of the hexane molecules remained in FR. As most of the migrated hexane molecules from FR get trapped in the G-NC and even after 5 ns they do not fully exit to the ER. The latter confirms the clogging of the nanochannel. The number of hexane molecule inside G-NC is almost 60 for both cases which gives the concentration of hexane molecules comparable to that of gas phase of hexane (see Figure 7(b)), i.e. 650 $\mathrm{Kgm^{-3}}$.

Now the question is how we can clean this contaminated nanochannel. To answer this question, we studied the effects of pressure and temperature on the clogging/unclogging of nanochannels for h=0.7 nm. The main results are presented in the next section and some complementary results are given in the supporting information (Figures S2 to S3). In fact, we apply pressure on the G-NC by moving the left graphene wall to the right side of the

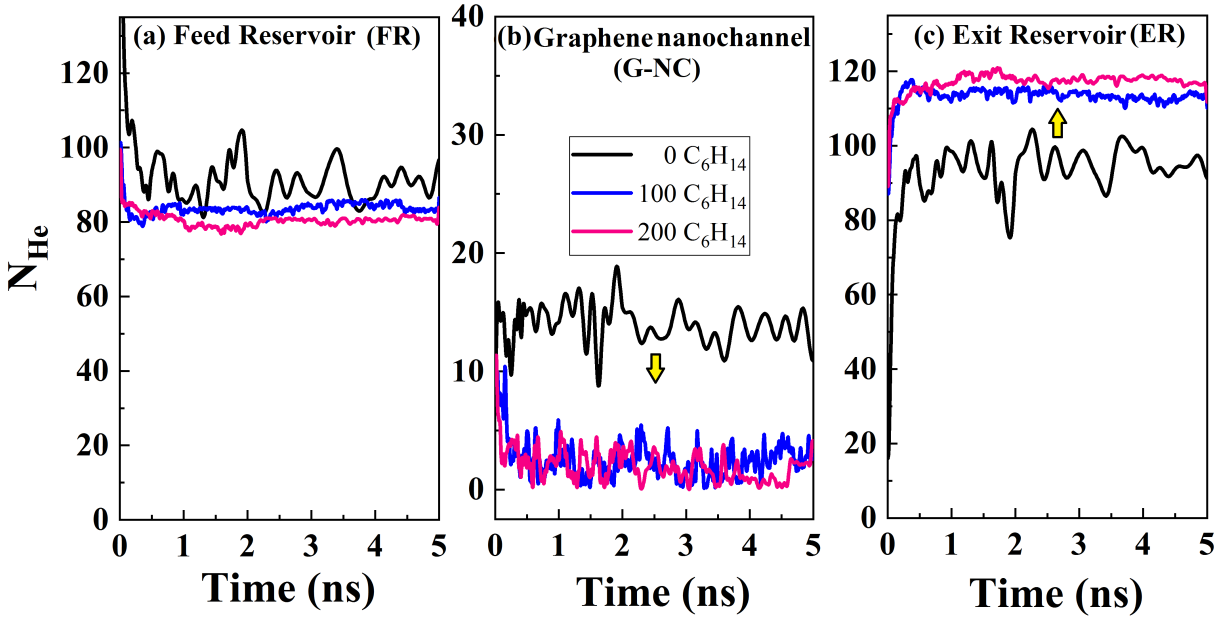

Figure 4: The time evolution of total number of He atoms in the (a) feed reservoir (FR), (b) graphene nanochannel (G-NC) and (c) exit reservoir (ER) for different number of hexane molecules. The results are averaged over a time interval of 5 ns. The nanochannel height is 0.7 nm. The yellow arrows refer to increasing (b) and decreasing (c) of the helium contents in G-NC and ER when the channels are exposed to hexane moelecules, respectively.

simulation box at a speed of 0.5 m/s. Using this method, the pressure of gas increases in the FR. However, as we see from Figure S3 and S4, applying this amount of pressure (≈ 0.3 bar) does not change the number of helium atoms and hexane molecules in FR, G-NC and ER. This is in very good agreement with experiment[17]

On the other hand the results of Sajja *et al.*[17] revealed that increasing the temperature up to 420 K can partially unclog the G-NC. We also studied the effects of temperature for unclogging and found that only few percent of stayed hexane molecules inside GNC are removed (see Figs. S4 and S5) which is aslo consistent with the results of Sajja *et al.*[17] In fact, the temperature enhancement led to the migration of some hexane molecules from the G-NC regions to FR and ER, which resulted in decreasing the number of hexane molecules in the G-NC (see Figure S5(b)). However, the number of He inside G-NC does not noticeably change (see Figure S4(b)). More details can be found in the supporting information.

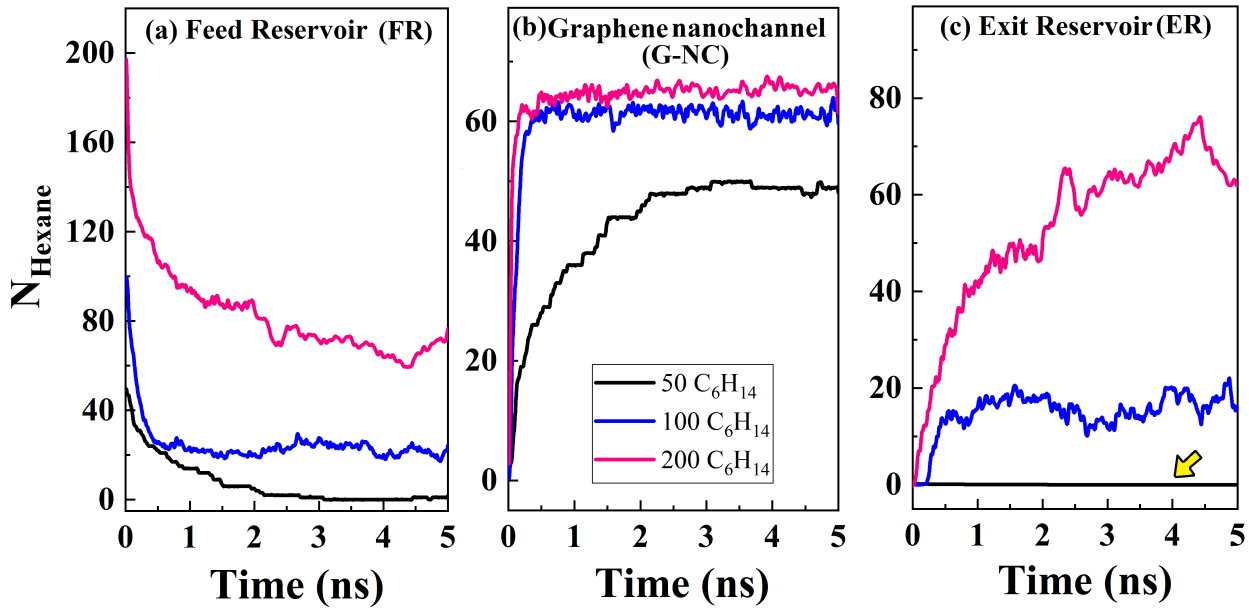

Figure 5: The The time evolution of total number of Hexane molecules in the a) feed reservoir (FR), b) graphene nanochannel (G-NC), and c) exit reservoir (ER). The results are averaged over a time interval of 5 ns. The nanochannel height is 0.7 nm. The yellow arroe in (c) shows zero tranported hexane molecule to the ER for low concentration case.

III.d. The graphene nanochannel size effects on the clogging/unclogging

Because in our simulations, increasing the number of hexane molecules larger than 200 does not influence the clogging effect (number of particles in the nanochannel remains unchanged), hereafter 1) only the results for 200 hexane molecules in the FR, and 2) the effects of channel size in the presence of helium gas based on the model-II are reported below. The nanochannels are simulated by removing n=1 to 5 layers from the layered graphene structure, which correspond to h=0.4, 0.7, 1.0, 1.4, and 1.7 nm, respectively (these are the channel size fabricated in the experiment[17]). Note that the simulation procedure is the same as that of the 0.7 nm nanochannel.

In Figures 6 and 7, we show the most important results of this work which are the change in relative density of He and hexane (ρ_{Hexane}) in the G-NC for different heights of nanochannel, respectively. Notice that the variation of D_r (see method) in the FR cannot

be used to determine clogging/unclogging nanochannels. Because when the number of He atoms in the FR decreases, some of them move to the G-NC and ER, as well as sometimes He atoms return to the FR. Therefore, we mostly focus on the D_r in the G-NC and ER regions. Also, for hexane flow through nanochannels, the density of hexane (ρ_{Hexane}) is a more relevant parameter.

III.e. The variation of helium density after exposure to hexane through various nanochannels: h=0.4 nm

As seen from Figures 6 and 7, at 300 K, when 200 hexane molecules are in the FR, the density of He atoms in the G-NC with a height of 0.4 nm is about 3.5 times larger than the initial density of He (see Figure 6(a)), while ρ_{Hexane} is zero (see Figure 7(a)), i,e, the nanochannels with h=0.4 nm do not allow hexane molecules to enter. In this case, an increase in the pressure in the FR push He atoms to be entered the G-NC and increasing ρ_{He}. Additionally, graphene wall motion (see gray bars in Figures 6 and 7) or increasing temperature (see orange bars in Figures 6 and 7) do not push hexane molecules to the 0.4 nm G-NC, but instead result in the partial transfer of He atoms to the ER region due to the increased kinetic energy of He atoms in the G-NC. As a consequence, as the temperature increases and FR volume decreases, D_r in the G-NC decreases and the number of He atoms in the ER increases. Moreover, as the G-NC does not contain hexane molecules (see Figure 7(a)), the increase in the ER does not imply the revival of flow in nanochannels. All of these observations are in excellent agreement with experiment.

III.f. The variation of helium density after exposure to hexane through various nanochannels: h=0.7 nm

For comparison purposes, here we investigate the flow of He atoms and hexane molecules in a nanochannel with a height of 0.7 nm that has been studied by details in the previous section. The results are shown in Figures 6(b) and 7(b), for He and hexane, respectively. At 300 K for h = 0.7 nm, the ρ_{Hexane} in the 0.7 nm G-NC is larger than the other nanochannels with h> 1 nm. Upon movement of the graphene walls, the density of particles in nanochannels

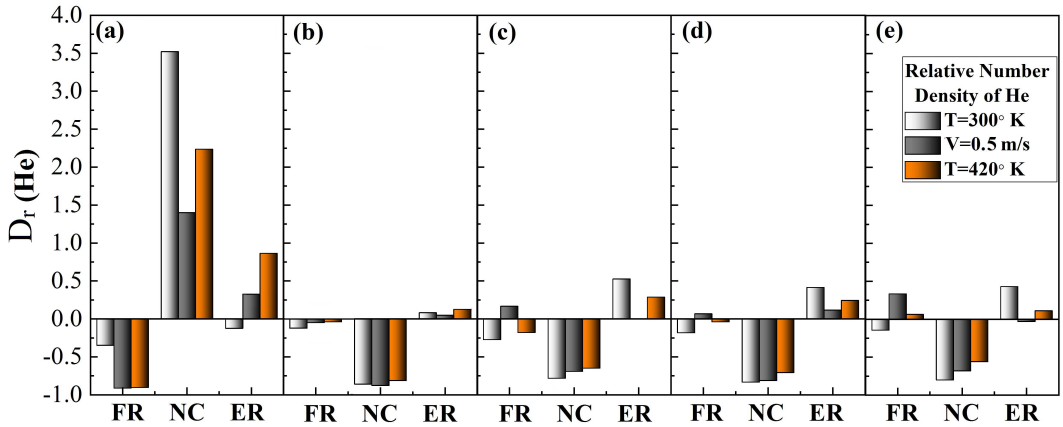

Figure 6: The relative density of He atoms (D_r) in the feed reservoir (FR), nanochannel (NC) and exit reservoir (ER) of graphene nanochannel with (a) h $=0.4$ nm, (b) h $=0.7$ nm, (c) h $=1.0$ nm, (d) h $=1.4$ nm and (e) h $=1.7$ nm.

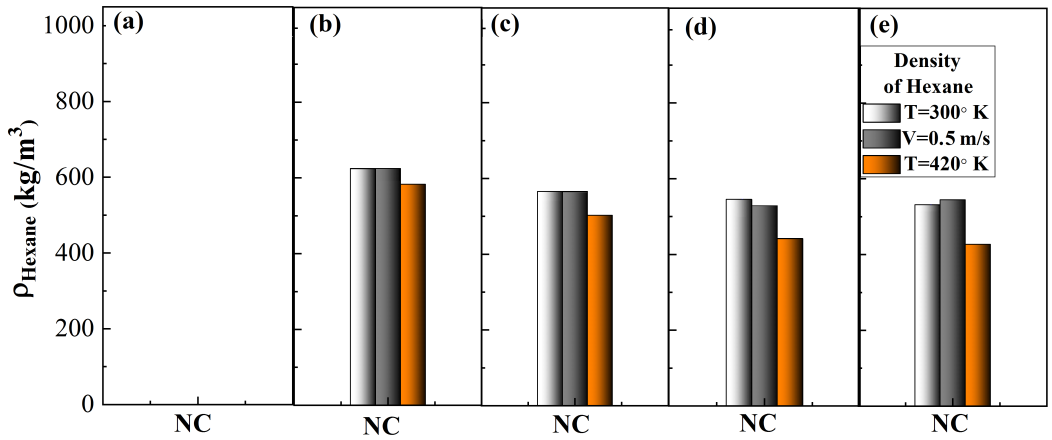

Figure 7: The density of hexane molecules (ρ_{Hexane}) in NC of graphene nanochannel with (a) h $=0.4$ nm, (b) h $=0.7$ nm, (c) h $=1.0$ nm, (d) h $=1.4$ nm and (e) h $=1.7$ nm.

with a height of 0.7 nm remains unchanged. Although the interaction between the hexane molecules and the G-NC is reduced by increasing the temperature and some hexanes transfer to the ER, the D_r in the G-NC and the ER does not vary significantly (see Figure 7). This result relates to the clogging in the 0.7 nm nanochannel, which agrees well to the experimental finding.[17]

III.g. The variation of helium density after exposure to hexane through various nanochannels: h>0.7 nm

Further, by increasing the height of the nanochannel at 300 K, ρ_{Hexane} (see Figure 7(c,d)

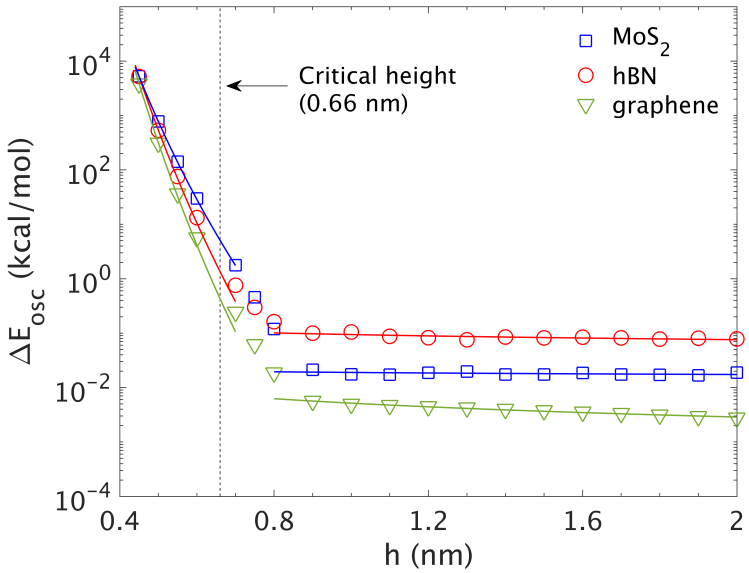

Figure 8: Oscillation amplitude of potential energy versus the channel height for graphene, hBN and MoS_2 nanochannels when hexane enters the nanochannel. The amplitudes decrease significantly with increasing channel height up to the vicinity of the critical height (indicated by vertical dashed line) after which an almost constant value is observed. Solid lines are power law functions fitted to the data.

white bars) and D_r (see Figure 6(s,d) white bar) within the G-NC are slightly reduced and increased, respectively. Accordingly, the clogging in the nanochannel with h >1 nm is less severe than the clogging in the channel with h = 0.7 nm. In many studies the influence of nanochannel height and dimensions on mass transfer were conducted. For example, Jiang *et al.*[27] investigated the relationship between the height of nanochannels and mass transfer in dense methane nanofluids. They found that the diffusion coefficients increase with the height of the nanochannel and reaches 80% of the bulk value when the nanochannel height is 20 times larger than the diameter of the methane molecules.

III.h. Effect of different nanochannel. In this section, the influence of the nanochannel material on the uptake of hexane molecule is studied by considering four different type of materials for nanochannels, i.e, graphene, hBN, BC_2N and MoS_2.

E*nergy barrier.* First, using model-I, in the previous section the different energy barriers for various channel heights made of different materials were discussed (see Figure 3). In

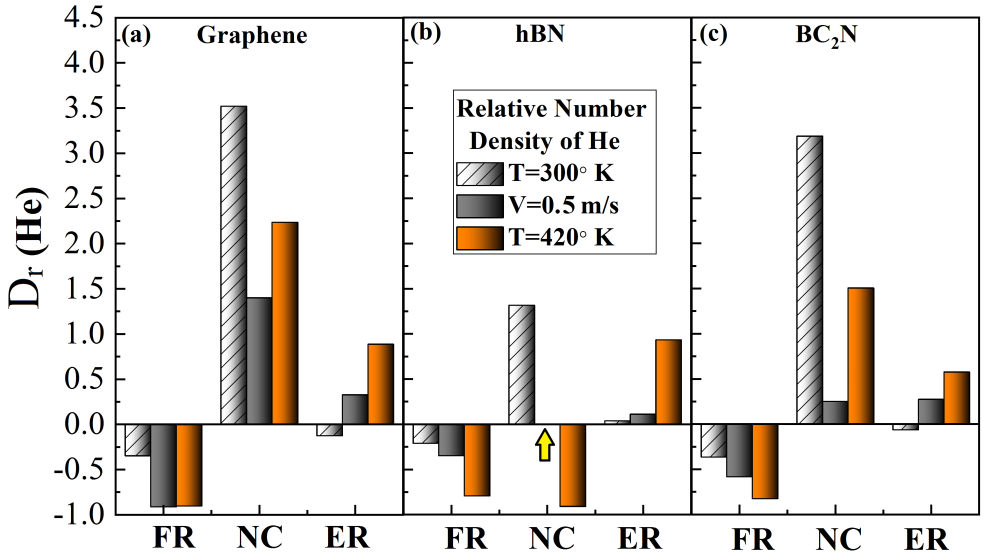

Figure 9: Relative density of He in FR, NC and ER of (a) graphene, (b) hBN and (c) BC_2N nanochannels with h= 0.4 nm. The yellow arrow in (b) indicate negligible change in the number of helium when the FR is subjected to the pressure by moving graphene walls.

a semi-logarithmic plot the corresponding variation of oscillation amplitude of potential energy (Δ) versus channel height is presented in Figure 8. Different materials explicitly show different oscillations amplitude. It is seen that the results for the hBN-NC and the MoS_2-NC exhibit larger fluctuations compared to those of the G-NC. Considering the lower energies, the unclogging of the hBN-NC and the MoS_2-NC appears to be more difficult than that of the G-NC, which is a distinct signature of long-range electrostatic forces on the above two nanochannel walls. Comparing the unclogging effects reported for the h=0.4 nm and the h=0.7 nm channels, although none of them responded to He flushing, the h=0.4 nm nanochannel has been unclogged after thermal annealing, while it is not the case for the h=0.7 nm nanochannel.[17] This is specifically noteworthy as it is against the trends of energy oscillation amplitude depicted in Figure 8.

The density of He/hexane. Second, we now turn our attention to the density of He/hexane in nanochannels made of different materials. Figure 9 shows the relative density of helium (D_r, see method) in the G-NC, the hBN-NC, and the BC_2N-NC at 0.4 nm height. Note that since the distance between two layers of MoS_2 structure is estimated to be between

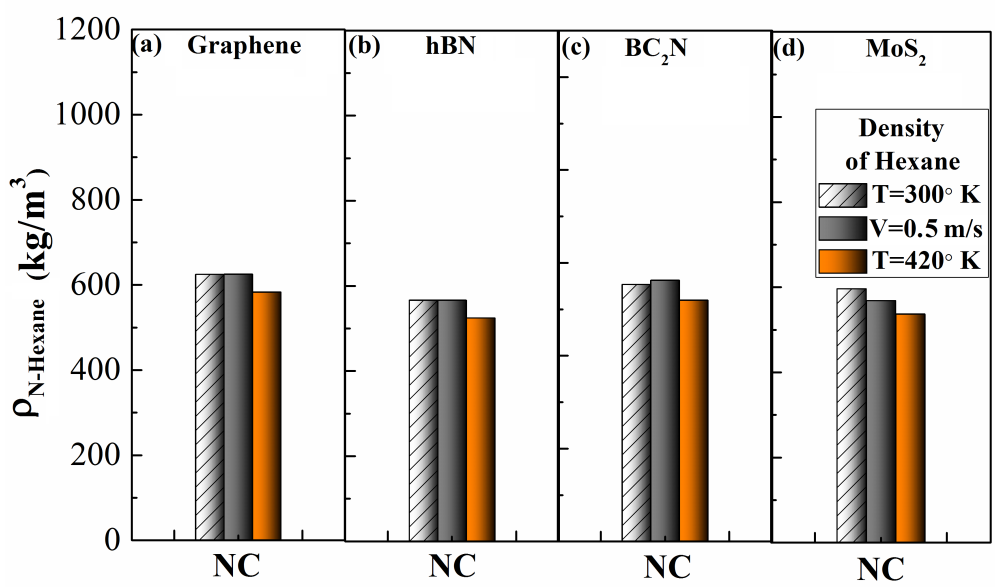

Figure 10: The same as Figure 7 but now for h= 0.7 nm.

h=0.6 nm and 0.7 nm,[28] there is no MoS_2 channel with h=0.4 nm. As a result of the tinny space within inside the channels resulting in the adsorption of He atoms by carbon by the nanochannels wall,[29] the D_r increased more than three times in the G-NC and the BC_2N-NC as compared to the initial density of He in the FR. In contrast, D_r in the hBN-NC is smaller than ρ_0 because, despite hexane, the hBN-NC absorbs fewer He atoms than the G-NC. At 300 K, after adding hexane molecules to the simulation box and increasing the pressure in the FR, approximately 30% of the He atoms are moved to the ER, and this behavior with larger percentage of passed helium is observed for different materials with h=0.4 nm. Notice that in Figures 6-10 V= 0.5 m/s means that the left and right graphene walls move to the right at a speed of 0.5 m/s for 5 ns with a time step of 1 fs at 300 K.

The ρ_{Hexane} in the different nanochannels with h = 0.7 nm (G-NC, hBN-NC, BC_2N-NC, and the MoS_2-NC) and the D_r in three regions of ER, nanochannel, and FR are shown in Figures 10 and 11. The G-NC clogging has been described previously which can be generalized to investigate clogging in other nanochannels. Increasing temperature causes an increase in D_r in the ER region. This is attributed to the enhancement of kinetic energy of the system which results in the transfer of He atoms from the nanochannel to the ER.

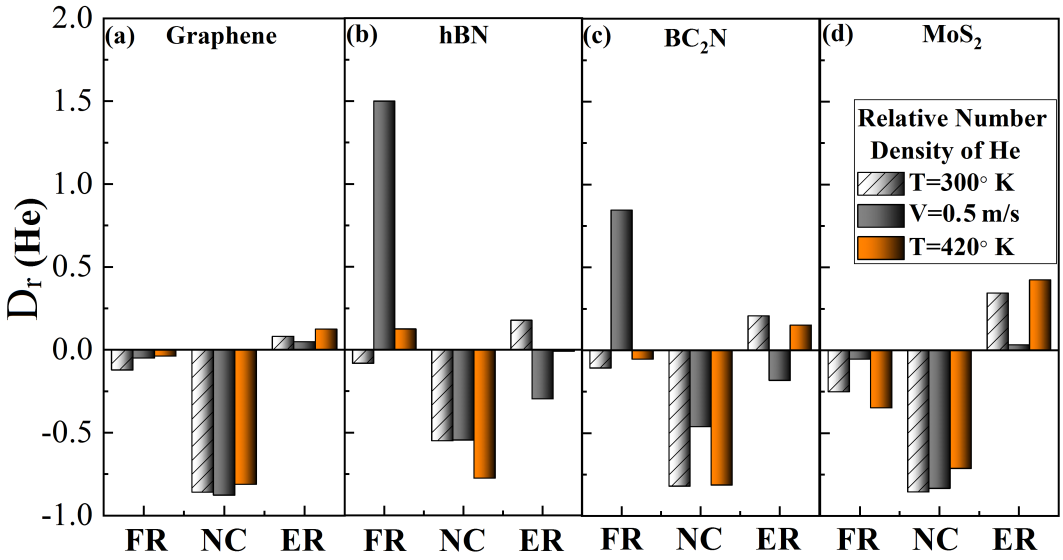

Figure 11: The same as Figure 9 but now for h= 0.7 nm.

As a result, despite increasing temperature the clogging of all the studied nanochannels is consistent with the experiment, and the number of hexane molecules in the nanochannel does not change significantly with changing pressure.

Hexane adsorption to the channel walls. Here by using model I, we calculate potential energy versus nanochannel height for hexane molecule at room and low temperature (5 K) where the corresponding results are shown in Figure S6. It is worth noting that, we repeated the simulation once more, and this time inversely started with the 2 nm nanochannel and gradually decreased the height and picked the smaller energy resulted from schemes of either opening up or narrowing the channel. Furthermore, the origin of the system potential energy was set to when the hexane was away from the nanochannel.

Noticeably, the curves exhibit minimum values close to the critical height for all nanochannels and for both temperature values suggesting that residing of the hexane molecule inside the channels is energetically highly favourable for channels of height around the critical value. On the contrary, for ultra slim channels the situation of the hexane inside the nanochannel is highly unstable. This may be the reason that in the experiments thermal annealing was not sufficient to get the hexane fully out of its favourable energy valley in the h=0.7 nm

nanochannel.[17]

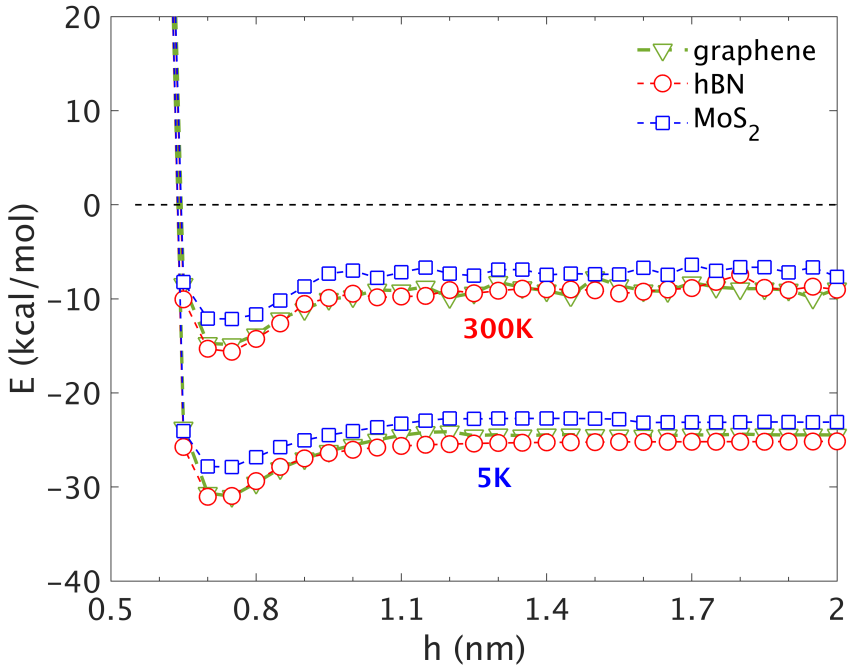

Figure 12: The systems potential energy versus the channel height. Around the critical height, the energy values exhibit a minimum making unclogging of the channels highly difficult. The E=0 crossing occurs for h = 0.64 nm and the minimum is found for h ≈ 0.7 nm.

Unclogging efficiency. Next, another noteworthy issue is the unclogging efficiency of the channels. In the experiment,[17] in wide channels even after several He flushing and annealing efforts, the channels were not completely unclogged and there was always some percentage of deficiency in their revival. It is specifically notable as the amplitude of energy fluctuations was not that significant (see Figure 8).

To interpret this, with the help of our MD trajectories, we found that hydrocarbon molecules in wide channels make bonds to one of the channel walls. Figure 12 depicts vertical distance between the hexane centre of mass and one of the channel walls versus the channel height for the graphene nanochannel. The results for the hBN and MoS_2 nanochannels are similar and are shown in Figures S7 and S9. The hexane molecule leaves the center of the channel for h = 0.9 nm when T = 5 K (this value increases to h = 1 nm for T = 300 K). The

figure shows that with increasing channel height the hexane bonds to one of the channel walls as can also be understand from the potential profiles shown in the inset of Figures S6-S8 for three different values of h . Moreover, as expected, bonding to one of the walls occurs beyond the critical height at low temperature which is related to the minimum energy point of Figure 12. At room temperature, however, thermal fluctuations shifts this to larger h-values. We interpret this as a result of thermal setting in MD which gives kinetic energy to the hexane hindering its binding to the wall.

Because of recent advantages in the fabrication of Å-scale channels, further studies are needed for elucidating the clogging/unclogging of hydrocarbon contaminated nanochannels using either molecular dynamics simulations or density functional theory calculations.

CONCLUSIONS

To conclude, using molecular dynamics simulations and energetic consideration, we investigated the contamination of the G-NC, the hBN-NC and the MoS_2-NC when exposed to hydrocarbon molecules. The nanochannel height is found to play a critical role in repelling or attracting the hydrocarbon towards entering the channel. Channels with a height smaller than the kinetic diameter of the contaminants cannot clog ($h < 0.4\,nm$). Nanochannels of height $h = 0.7\,nm$ is found to be an energetically favourable channel for uptake hydrocarbon molecule. The hydrocarbon bonds to one of the channel walls making the nanochannel's unclogging inaccessible. The increase in temperature can partially unclog the channel with $h = 0.7\,nm$, while the increase in pressure has no significant effects on the unclogging of this channel. However, we found that, for channels with $h > 1\,nm$, increasing temperature and pressure clean the channels. Also, for channels made of different materials, the He flow changes slightly and the wall material has smaller effects as compared to the effects of the height of the channel. We conclude that the potential field induced by the nanochannel wall and especially the height of the nanochannel governs the clogging and unclogging of the

nanochannels. Our results are consistent with the recent experiment and give deeper insights into the underlying physics of the problem[17] and will open a new avenue in the research of clogging/unclogging of hydrocarbon contaminated nanochannels.

METHODS

Two types of simulations are performed using the Large-scale Atomic/Molecular Massively Parallel Simulator (LAMMPS) Package.[30] In the simulations corresponding to the first model, the hexane and cyclohexane molecules are simulated using the OPLS potential van der Waals and electrostatic interactions have been considered between the hydrocarbon molecule and the walls. Van der Waals interactions are estimated using the Lennard-Jones (LJ) potential. Table 1 summarises the LJ coefficients, as well as the electrostatic charges of the particles. The LJ cross parameters are estimated using the Lorentz-Bertholet mixing rule. Particle-particle-particle-mesh algorithm is implemented for calculating the long range electrostatic forces in k-space. Newtonian equations of motion are integrated using velocity-verlet algorithm with a time-step of 0.5 fs. The simulations are performed in canonical ensemble (NVT) using Nose-Hoover thermostat. All calculations are carried out using the LAMMPS package.

For the second set of simulations in order to handle the interaction between helium atoms and hydrocarbons, the hexane molecules are modeled using an adaptive intermolecular reactive bond order (AIREBO)[31] potential. The repulsive and attractive pair interaction are both modified to fit the bond properties, the long-range atomic interactions, and the torsional interactions between single bonds. The van der Waals and electrostatic interactions have been considered between the hydrocarbon molecule and the walls. The van der Waals interactions are estimated using the Lennard-Jones (LJ) potential.[32] A cut-off of 1.2 nm is used to include short-range interactions.

Table 1 summarizes the LJ coefficients. The LJ cross parameters are estimated using the

Lorentz-Bertholet mixing rule. Particle-particle-particle-mesh algorithm[33] is implemented for calculating the long range electrostatic forces in k-space. The Newtonian equations of motion are integrated using the velocity-verlet algorithm. The simulations are performed within the canonical ensemble (NVT) using Nosé-Hoover thermostat. In order to determine the possible flow of hexane in different channels that have different heights, the He atoms are relaxed during 5 ns with a time step of 1 fs, and then two different simulations are run:

(1) The penetration of hexane molecules and the clogging of the nanochannel are studied for 5 ns with a time step of 1 fs at 300 K, then the left and right graphene walls move to the right at a speed of 0.5 m/s for 5 ns with a time step of 1 fs.

(2) The entry of hexane molecules and the clogging in the nanochannel are studied at 420 K. The experimental results of Sajja *et al.*[17] revealed that increasing the temperature up to 420 K can partially unclog the G-NC. The latter is performed for 5 ns with a time-step of 1 fs.

Table 1: The potential parameters used in our MD simulations.

interaction type	ϵ (eV)	σ (nm)	q_i (e)	Ref.
He	0.0009	0.26	0	[29]
C (Hexane)	0.0028	0.34	-0.06	[31,34]
H (Hexane)	0.0014	0.26	+0.06	[31,34]
C	0.0024	0.38	0	[35]
B	0.0041	0.34	+0.3	[36]
N	0.0026	0.34	-0.3	[36]
Mo	0.0024	0.36	+0.76	[37]
S	0.011	0.27	-0.38	[37]

The relative density (D_r) is used to analyze the change in flow of He atoms in the G-NC as follows:

$$D_r = (\rho - \rho_0)/\rho_0 = (N - N_0)/N_0, \tag{1}$$

where, $\rho(N)$ and $\rho_0(N_0)$ refer to the density (number) of He atoms, before and after the addition of hexane molecules in the simulation box, respectively. Notice that when $\rho < \rho_0$,

then the obtained values of D_r are negative. This is when the particles migrate from their first region (FR, NC, ER) to the other regions. In other words, the number of particles in a region in the initial step is less than the equilibrium number.

Acknowledgement

N. Hassani and Z. Javdani acknowledge ISEF support. Part of this work was supported by FWO-Vlaanderen. The computational resources used in this work were provided by the HPC core facility CalcUA of the Universiteit Antwerpen, and VSC (Flemish Supercomputer Center), by the Research Foundation Flanders (FWO) and the Flemish Government.

Supporting Information Available

Variation of the system potential energy for the cyclohexane molecule in different nanochannels (Figure S1). The effect of the pressure on the total number of He/hexane atoms/molecules in FR, G-NC, and ER in the 0.7 nm graphene nanochannel (Figures S2 and S3). The effect of the temperature on the total number of hexane molecules in FR, G-NC, and ER in the 0.7 nm graphene nanochannel (Figures S4 and S5). Vertical distance between the hexane centre of mass and one of the channel walls versus the channel height of graphene, hBN, and MoS_2 (Figures S6-S8).

References

(1) Hibara, A.; Saito, T.; Kim, H.-B.; Tokeshi, M.; Ooi, T.; Nakao, M.; Kitamori, T. Nanochannels on a fused-silica microchip and liquid properties investigation by time-resolved fluorescence measurements. *Analytical Chemistry* **2002**, *74*, 6170–6176.

(2) Sparreboom, W.; van den Berg, A.; Eijkel, J. C. Principles and applications of nanofluidic transport. *Nature Nanotechnology* **2009**, *4*, 713–720.

(3) Fornasiero, F.; Park, H. G.; Holt, J. K.; Stadermann, M.; Grigoropoulos, C. P.; Noy, A.; Bakajin, O. Ion exclusion by sub-2-nm carbon nanotube pores. *Proceedings of the National Academy of Sciences* **2008**, *105*, 17250–17255.

(4) Siria, A.; Poncharal, P.; Biance, A.-L.; Fulcrand, R.; Blase, X.; Purcell, S. T.; Bocquet, L. Giant osmotic energy conversion measured in a single transmembrane boron nitride nanotube. *Nature* **2013**, *494*, 455–458.

(5) Secchi, E.; Marbach, S.; Niguès, A.; Stein, D.; Siria, A.; Bocquet, L. Massive radius-dependent flow slippage in carbon nanotubes. *Nature* **2016**, *537*, 210–213.

(6) Secchi, E.; Niguès, A.; Jubin, L.; Siria, A.; Bocquet, L. Scaling behavior for ionic transport and its fluctuations in individual carbon nanotubes. *Physical Review Letters* **2016**, *116*, 154501.

(7) Tunuguntla, R. H.; Henley, R. Y.; Yao, Y.-C.; Pham, T. A.; Wanunu, M.; Noy, A. Enhanced water permeability and tunable ion selectivity in subnanometer carbon nanotube porins. *Science* **2017**, *357*, 792–796.

(8) Garaj, S.; Hubbard, W.; Reina, A.; Kong, J.; Branton, D.; Golovchenko, J. Graphene as a subnanometre trans-electrode membrane. *Nature* **2010**, *467*, 190–193.

(9) Joshi, R.; Carbone, P.; Wang, F.-C.; Kravets, V. G.; Su, Y.; Grigorieva, I. V.; Wu, H.; Geim, A. K.; Nair, R. R. Precise and ultrafast molecular sieving through graphene oxide membranes. *Science* **2014**, *343*, 752–754.

(10) Jain, T.; Rasera, B. C.; Guerrero, R. J. S.; Boutilier, M. S.; O'hern, S. C.; Idrobo, J.-C.; Karnik, R. Heterogeneous sub-continuum ionic transport in statistically isolated graphene nanopores. *Nature Nanotechnology* **2015**, *10*, 1053–1057.

(11) Feng, J.; Graf, M.; Liu, K.; Ovchinnikov, D.; Dumcenco, D.; Heiranian, M.; Nandi-

gana, V.; Aluru, N. R.; Kis, A.; Radenovic, A. Single-layer MoS_2 nanopores as nanopower generators. *Nature* **2016**, *536*, 197–200.

(12) Hong, S.; Constans, C.; Surmani Martins, M. V.; Seow, Y. C.; Guevara Carrio, J. A.; Garaj, S. Scalable graphene-based membranes for ionic sieving with ultrahigh charge selectivity. *Nano Letters* **2017**, *17*, 728–732.

(13) Abraham, J.; Vasu, K. S.; Williams, C. D.; Gopinadhan, K.; Su, Y.; Cherian, C. T.; Dix, J.; Prestat, E.; Haigh, S. J.; Grigorieva, I. V., et al. Tunable sieving of ions using graphene oxide membranes. *Nature Nanotechnology* **2017**, *12*, 546–550.

(14) Hummer, G.; Rasaiah, J. C.; Noworyta, J. P. Water conduction through the hydrophobic channel of a carbon nanotube. *Nature* **2001**, *414*, 188–190.

(15) Majumder, M.; Siria, A.; Bocquet, L. Flows in one-dimensional and two-dimensional carbon nanochannels: Fast and curious. *MRS Bulletin* **2017**, *42*, 278–282.

(16) Chen, X.; Yang, Z.; Feng, S.; Golbek, T. W.; Xu, W.; Butt, H.-J.; Weidner, T.; Xu, Z.; Hao, J.; Wang, Z. How universal is the wetting aging in 2D materials. *Nano Letters* **2020**, *20*, 5670–5677.

(17) Sajja, R.; You, Y.; Qi, R.; Goutham, S.; Bhardwaj, A.; Rakowski, A.; Haigh, S.; Keerthi, A.; Radha, B. Hydrocarbon contamination in angstrom-scale channels. *Nanoscale* **2021**, 9553–9560.

(18) Koshino, M.; Solin, N.; Tanaka, T.; Isobe, H.; Nakamura, E. Imaging the passage of a single hydrocarbon chain through a nanopore. *Nature Nanotechnology* **2008**, *3*, 595–597.

(19) Chow, P. K.; Singh, E.; Viana, B. C.; Gao, J.; Luo, J.; Li, J.; Lin, Z.; Elías, A. L.; Shi, Y.; Wang, Z., et al. Wetting of mono and few-layered WS_2 and MoS_2 films supported on Si/SiO_2 substrates. *ACS Nano* **2015**, *9*, 3023–3031.

(20) Fujimoto, T.; Takeda, K.; Nonaka, T. *Developments in Surface Contamination and Cleaning*; Elsevier, 2008; pp 329–474.

(21) Nourbakhsh, A.; Cantoro, M.; Klekachev, A.; Clemente, F.; Soree, B.; Van Der Veen, M.; Vosch, T.; Stesmans, A.; Sels, B.; De Gendt, S. Tuning the fermi level of SiO2-supported single-layer graphene by thermal annealing. *The Journal of Physical Chemistry C* **2010**, *114*, 6894–6900.

(22) Haigh, S. J.; Gholinia, A.; Jalil, R.; Romani, S.; Britnell, L.; Elias, D. C.; Novoselov, K. S.; Ponomarenko, L. A.; Geim, A. K.; Gorbachev, R. Cross-sectional imaging of individual layers and buried interfaces of graphene-based heterostructures and superlattices. *Nature materials* **2012**, *11*, 764–767.

(23) Li, J.; Rao, Q.; Xia, Y.; Hoepfner, M.; Deo, M. D. Confinement-mediated phase behavior of hydrocarbon fluids: Insights from Monte Carlo simulations. *Langmuir* **2020**, *36*, 7277–7288.

(24) Qu, H.; Rayabharam, A.; Wu, X.; Wang, P.; Li, Y.; Fagan, J.; Aluru, N. R.; Wang, Y. Selective filling of n-hexane in a tight nanopore. *Nature Communications* **2021**, *12*, 1–8.

(25) Keerthi, A.; Geim, A.; Janardanan, A.; Rooney, A.; Esfandiar, A.; Hu, S.; Dar, S.; Grigorieva, I.; Haigh, S.; Wang, F., et al. Ballistic molecular transport through two-dimensional channels. *Nature* **2018**, *558*, 420–424.

(26) Aguilar-Armenta, G.; Dıaz-Jiménez, L. Characterization of the porous structure of two naturally occurring materials through N_2-adsorption (77 K) and gas chromatographic methods. *Colloids and Surfaces A: Physicochemical and Engineering Aspects* **2001**, *176*, 245–252.

(27) Jiang, C.; Wang, X.; Liu, Q.; Wang, X.; Ke, C. Investigation of the relationship between

nanochannel width and mass transfer characteristics for dense methane nanofluidics. *International Communications in Heat and Mass Transfer* **2020**, *118*, 104879.

(28) Xiao, J.; Long, M.; Li, X.; Zhang, Q.; Xu, H.; Chan, K. Effects of van der Waals interaction and electric field on the electronic structure of bilayer MoS_2. *Journal of Physics: Condensed Matter* **2014**, *26*, 405302.

(29) Ghasemzadeh, H.; Babaei, S.; Tesson, S.; Azamat, J.; Ostadhassan, M. From excess to absolute adsorption isotherm: The effect of the adsorbed density. *Chemical Engineering Journal* **2021**, *425*, 131495.

(30) Plimpton, S. Fast parallel algorithms for short-range molecular dynamics. *Journal of Computational Physics* **1995**, *117*, 1–19.

(31) Stuart, S. J.; Tutein, A. B.; Harrison, J. A. A reactive potential for hydrocarbons with intermolecular interactions. *The Journal of chemical physics* **2000**, *112*, 6472–6486.

(32) Lim, T.-C. The relationship between Lennard-Jones (12-6) and Morse potential functions. *Zeitschrift für Naturforschung A* **2003**, *58*, 615–617.

(33) Hockney, R. W.; Eastwood, J. W. *Computer simulation using particles*; Crc Press, 2021.

(34) Jorgensen, W. L.; Madura, J. D.; Swenson, C. J. Optimized intermolecular potential functions for liquid hydrocarbons. *Journal of the American Chemical Society* **1984**, *106*, 6638–6646.

(35) Girifalco, L. A.; Hodak, M.; Lee, R. S. Carbon nanotubes, buckyballs, ropes, and a universal graphitic potential. *Physical Review B* **2000**, *62*, 13104.

(36) Wagemann, E.; Wang, Y.; Das, S.; Mitra, S. K. On the wetting translucency of hexagonal boron nitride. *Physical Chemistry Chemical Physics* **2020**, *22*, 7710–7718.

(37) Hu, C.; Yi, C.; Bai, M.; Lv, J.; Tang, D. Molecular dynamics study of the frictional properties of multilayer MoS_2. *RSC Advances* **2020**, *10*, 17418–17426.

TOC Graphic

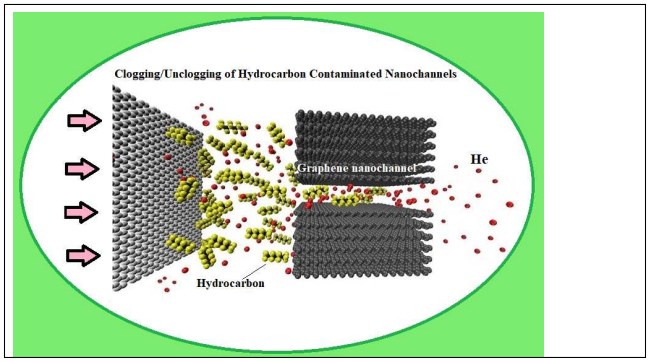
Clogging/Unclogging of Hydrocarbon Contaminated Nanochannels
Graphene nanochannel
He
Hydrocarbon